

FAULT-TOLERANT MATCHED-FIELD PROCESSING IN THE PRESENCE OF ELEMENT FAILURES

KILSEOK CHO, ALAN D. GEORGE, AND RAJ SUBRAMANIYAN

High-performance Computing and Simulation (HCS) Research Laboratory

Department of Electrical and Computer Engineering, University of Florida

P.O. Box 116200, Gainesville, FL 32611-6200

KEONWOOK KIM

Department of Electronics Engineering, Dongguk University

3-26 Pil-Dong Chung-Gu, Seoul 100-715, Korea

Received 20 February 2004

Revised 16 May 2005

In the highly cluttered undersea environment, sonar array systems require enhanced acoustic signal processing algorithms and sophisticated architectures in order to meet dependability and real-time mission requirements. The probability of hydrophone and processing element failures is very high in such severe operating environments. Adaptive matched-field processing (MFP) algorithms localize sources accurately with moderate levels of signal-to-noise ratio and precise knowledge about environments by employing full-wave acoustic propagation models. However, they highly distort output beam patterns with significant increase of sidelobes in the presence of environmental mismatches and element failures. These problems make the development of advanced fault-tolerant signal processing algorithms imperative to tolerate the element failures in cases where replacement of defective elements is impossible or impractical. In this paper, three fault-tolerant MFP algorithms are presented to compensate for the performance degradation generated by the inherent failure characteristics of vertical line arrays. The beamforming performance and computational complexities for these fault-tolerant algorithms are analyzed in terms of the number of faulty elements, their positions in the array, and signal-to-noise ratios. The simulation results demonstrate that these fault-tolerant techniques provide a feasible solution for real-time and highly reliable beamforming implementation on sonar array systems.

1. Introduction

The minimum variance distortionless response MFP (MVDR-MFP) algorithm adaptively attempts to pass a signal received from the desired point with unity gain and suppresses signals arriving from all the other points¹. This adaptive MFP algorithm localizes the source more accurately than conventional MFP with moderate levels of signal-to-noise ratio (SNR) and precise knowledge about environments since it provides significant interference rejection and sidelobe suppression. In sonar array systems operating in severe undersea environments, the probability of sensor element failures is very high. Replacement of the defective elements is an impractical alternative to remedy the failure since it is too expensive and time-consuming. The element failures in the array are a source of significant performance degradation because the defective array presents either distorted or no pressure fields. Array failure correction using numerical algorithms instead of element replacement is a very challenging task due to the randomness of the problem elements and the desired beam pattern². The performance of the adaptive MFP algorithm is also seriously degraded by environmental mismatches such as incorrect ocean waveguide models because the ability of the correlation processor to accurately detect a source is considerably dependent upon these assumed

models. Thus, a good understanding of the effects of element failures on system performance is necessary to develop fault-tolerant MFP algorithms in the presence of element failures.

The defective elements of the sonar array cause a distorted beam pattern and a significant increase in sidelobe levels of the outputs for beamforming algorithms³. For plane-wave beamforming, such element failures create an increased sidelobe level whose peak value depends on the ratio of the sum of the weights of defective elements to the sum of the weights of operating elements⁴. Several plane-wave beamforming algorithms have been developed to tolerate defective elements as an alternative to element replacement⁵⁻⁷. For adaptive MFP algorithms, numerous research has been conducted to develop methods to compensate for the performance degradation generated by environmental and system mismatches. The multiple linear constraint beamformer was developed to obtain robustness to environmental uncertainties for the maximum likelihood MFP algorithm⁸. The reduced minimum variance beamformer has been employed to reduce performance degradation in the presence of phase and amplitude errors in acoustic environmental models for horizontal and vertical line arrays⁹. The reduced-rank methods have also been proposed for adaptive MFP algorithms in order to enhance stability in adaptive weight calculation when there are mismatches between measured signals and calculated signals or the number of available snapshots is limited^{10,11}. The methods reduce the dimension of the matrix to be inverted without significantly destroying the signal information. The sector-focused stability method provides stable source estimation performance and reduces computational cost in the presence of highly correlated modal noises¹². These adaptive MFP algorithms have extensively been used to improve robustness and performance by employing environmental perturbation constraints and dimensionality reduction on simulated and field data when system and environmental mismatches occur. However, research on a fault-tolerant MVDR-MFP algorithm has not previously been undertaken to compensate for the performance degradation presented by element failures.

In this paper, the impacts of this mismatch are analyzed to understand the effects of element failures on system performance. An analytical method is used for predicting the MFP output power level to the mismatch. Three fault-tolerant algorithms suitable for MVDR-MFP are presented and analyzed in terms of source detection performance and computational complexity to compensate for the performance degradation generated by the element failures. The first is the multiple-constraint MVDR matched-field processing (MCMVDR-MFP) algorithm. This algorithm achieves fault tolerance and retains satisfactory sidelobe control by employing multiple linear constraints to tolerate element failures. Multiple linear constraints are employed in order to have unity gain constraint for a desired point as in the MVDR algorithm and zero gain constraints for defective elements to mitigate the effects of the distorted data from defective elements. The second is the reduced-rank MVDR matched-field processing (RRMVDR-MFP) algorithm. RRMVDR-MFP obtains improved robustness by projecting the array output vectors onto a lower dimensional subspace while preserving signal vectors and filtering out noise vectors distorted by the defective element. The third is the compensated MVDR matched-field processing (CMVDR-MFP) algorithm. It uses an estimation algorithm to reconstruct the data from the faulty nodes with that from neighboring functioning elements. The MVDR-MFP algorithm is applied to obtain final beamforming outputs after interpolating the data for faulty nodes. The fault-tolerant MVDR-MFP algorithms will provide better performance than MVDR-MFP in the presence of element failures while slightly increasing their computational complexities compared to that of MVDR-MFP.

The performance of the three fault-tolerant algorithms is analyzed in terms of peak-to-background ratio and ambiguity surface. The sensitivity of the output power to the mismatch generated by element failures is investigated to evaluate the impact on detection performance in terms of signal-to-noise ratios, number of faulty elements, and their positions. Additionally, the computational complexities and execution times of

the fault-tolerant algorithms are also analyzed to determine if the algorithms are a feasible solution for real-time sonar array systems.

The rest of paper is organized as follows. Section 2 presents the effects of mismatch on the MVDR-MFP algorithm in the presence of element failures. Section 3 provides a theoretical background and describes features of the fault-tolerant algorithms. The computational complexities and execution times of the fault-tolerant algorithms are examined in Section 4 and their performance is analyzed in Section 5. Finally, Section 6 presents a brief set of conclusions.

2. Effects of Element Failures

The replica vectors of MFP are a complicated function of the environmental and system parameters. When knowledge of the system and environmental parameters including length of the array, sensor position, sound speed, frequency, water depth, and bottom shape is imprecise, the replicas predicted from the assumed knowledge and the observations received from the array of sensors do not match. If the replica does not closely match the actual signals that are propagated through the environment, the performance of the beamformer will be seriously degraded. The normal-mode propagation model used to obtain the replica vectors can be expressed mathematically in a straightforward manner. Thus, an analytical method for predicting the sensitivity of the output power level to replica mismatch is employed to examine the effects of element failures in the array.

The power ratio for a MFP beamformer, $\rho(\omega, \Theta)$, is defined as the ratio of the processor power response for a replica vector with mismatch over that for a replica vector without mismatch¹³. Here ω is angular frequency of the source and $\Theta = (r, z)^T$ is the source parameter vector which includes range r and depth z . The power ratio is evaluated at the peak points in the search region. The peak is located at or near the assumed position of the source. At a particular source position, $\Theta = \Theta_s$, the power ratio at the peak points is given by

$$\rho(\omega, \Theta_s) = \frac{S[\tilde{p}(\omega, \Theta_s)]}{S[p(\omega, \Theta_s)]} \quad (1)$$

where $S[\cdot]$ is the processor power response, $\tilde{p}(\omega, \Theta_s)$ is the normalized replica vector with mismatch, and $p(\omega, \Theta_s)$ is the normalized replica vector without mismatch. When there is no mismatch, $p(\omega, \Theta_s) = \tilde{p}(\omega, \Theta_s)$, the power ratio of MFP is unity, $\rho(\omega, \Theta_s) = 1$. The degree to which $\rho(\omega, \Theta_s)$ is less than one projects the effect of mismatch for a source at $\Theta = \Theta_s$. A lower power ratio means that the MFP beamformer achieves poorer performance due to this mismatch.

For the normal-mode signal replica vector, power ratios of conventional MFP (CMFP) and MVDR-MFP are derived by assuming that the additive noise is uncorrelated. The power ratios for CMFP and MVDR-MFP are expressed as

$$\rho_{CMFP}(\omega, \Theta_s) = 1 - \left(\frac{\alpha^2}{1 + \alpha^2} \right) \left(1 - |\tilde{p}^H(\omega, \Theta_s)p(\omega, \Theta_s)|^2 \right) \quad (2)$$

$$\rho_{MVDR}(\omega, \Theta_s) = \frac{1}{1 + \alpha^2 \left(1 - |\tilde{p}^H(\omega, \Theta_s)p(\omega, \Theta_s)|^2 \right)} \quad (3)$$

where α^2 is the signal-to-noise ratio, $\tilde{p}^H(\omega, \Theta_s)p(\omega, \Theta_s)$ is the inner product of the replica vector with mismatch and the replica vector with no mismatch, and H denotes the complex conjugate transpose. From the above equations, the impacts of sound-speed and sensor position errors on the detection performance of the MFP algorithms are quantified by the magnitude of inner product of the two replica vectors and the

signal-to-noise ratio¹³. The above expressions can also be used to analyze the power ratio due to the mismatch from element failures. In this analysis, the rows in the replica vector corresponding to faulty elements are zero since it is assumed that the array of sensors receives no pressure field from the defective elements.

The power ratio expressions are used to examine the impact of element failures on the CMFP and MVDR-MFP algorithms for a vertical line array containing 32 hydrophones which are spaced 3 m apart from 10 m to 103 m in depth. In this analysis, the pressure field data is generated by the Kraken normal mode model¹⁴ for a point source which has 200 Hz frequency and 10 propagating modes, and is located at 10 km in range and 60 m in depth. The noise component of each hydrophone has Gaussian distribution with zero mean and signal-to-noise ratio of 10 dB. In faulty-node configurations, the faulty nodes are distributed from the 10th node toward the bottom-end with a spacing of one. For example, if the number of faulty nodes is three, the 10th, 11th, and 12th nodes are defective in the vertical line array.

Fig. 1a shows that the impact of element failures in MVDR-MFP is greater than that in CMFP. The impacts on both algorithms are increased as the number of defective sensors increases. It can be seen from Fig. 1b that the power ratio rapidly decreases as signal-to-noise ratio increases since a high signal-to-noise ratio increases gain of the MVDR-MFP algorithm, resulting in increasing the effects of mismatch. The power ratio of MVDR-MFP is lower than that of CMFP since adaptive beamforming algorithms generally use certain assumptions to obtain better resolution and hence are more sensitive than conventional beamformers even though there is a small amount of mismatch in the assumed parameters. The power ratios of CMFP and MVDR-MFP are depicted in Fig. 1c, 1d, and 1e in terms of the positions of faulty nodes and the locations of a signal source. The effects of element failures vary slightly according to positions of the defective nodes and locations of the source. The impact of defective sensors located in strong pressure fields is higher than that of defective sensors located in weak pressure fields. For instance, the power ratio of a faulty configuration where there are defective elements in the 14th and 15th positions is the lowest in Fig. 1c. The reason is that the pressure fields received from these two sensors are the strongest according to the pressure field data generated by the acoustic propagation model for the given environmental and source parameters. Furthermore, the power ratio varies with the range and depth of the source because the pressure field intensity of each element varies with source positions.

3. Fault-tolerant MFP Algorithms

The MVDR-MFP algorithm, which adaptively calculates optimal weights or gains, localizes the source more accurately than CMFP with moderate levels of SNR and precise knowledge about environments since it provides significant noise rejection and sidelobe suppression. However, MVDR-MFP is sensitive to mismatches such as inaccurate knowledge of the environmental parameters and element failures. The mismatches generate perturbations in the cross-spectral matrix (CSM), causing the weight vector of MVDR-MFP to be susceptible to these mismatches. The three fault-tolerant MFP algorithms, MCMVDR, RRMVDR, and CMVDR, are presented in order to improve localization performance in the presence of element failures. The MCMVDR-MFP and RRMVDR-MFP algorithms adjust the weights or gains of the array to compensate for the performance degradation due to the element failures, while the CMVDR-MFP algorithm reconstructs the signals for defective elements by using a prediction algorithm that is applied to neighboring elements. In the following sections, the input data model for the array in the ocean waveguide and the three fault-tolerant algorithms are explained in detail.

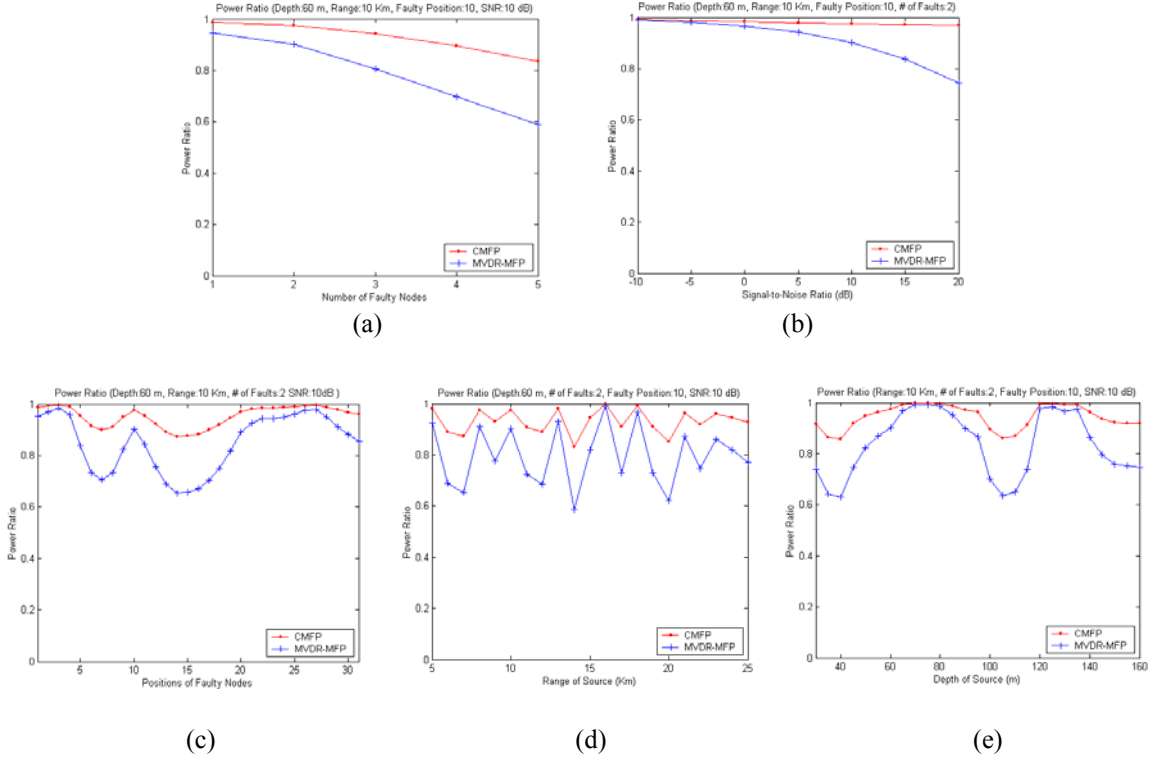


Fig. 1. Effects of element failures for CMFP and MVDR-MFP in terms of number of faulty nodes (a), SNR (b), position of faulty nodes (c), range of the source (d), and depth of the source (e).

3.1. Input data model

A data model for signals received from an underwater acoustic array composed of N sensors in the frequency domain is given by

$$x(\omega_n) = s(\omega_n)p(\omega_n, \Theta, \Psi) + n(\omega_n) \quad (4)$$

where $x(\omega_n)$ is the output vector of the N elements at frequency ω_n , $s(\omega_n)$ is the Fourier coefficient of the source data, and $n(\omega_n)$ is the noise vector at the frequency ω_n . The vector $p(\omega_n, \Theta, \Psi)$ is a replica vector calculated from the acoustic propagation model between the source located at $\Theta = (r_s, z_s)$ and the array, and Ψ represents the environmental parameters. The pressure field of the sensor placed at z_n from an acoustic source at position (r_s, z_s) is obtained using numerous acoustic models to solve the wave equation. The normal-mode model is used as the acoustic propagation model of the ocean because it provides an accurate and computationally efficient propagation model for MFP applications. The normal-mode method expresses the acoustic pressure field in terms of a normal-mode expansion and then solves for the eigenvalues and eigenfunctions of the wave equation. The acoustic pressure field at position (z_n) is the weighted sum of the contribution from each mode and can be calculated as

$$p(z_n; \Theta) \approx \frac{i}{\sqrt{8\pi r_s}} e^{-\frac{i\pi}{4}} \sum_{m=1}^{\infty} \varphi_m(z_s) \varphi_m(z_n) \frac{e^{ik_m r_s}}{\sqrt{k_m}} \quad (5)$$

where eigenfunction $\varphi_m(z)$ and eigenvalue k_m^2 are the mode shape function and horizontal wave number for mode m , respectively¹⁵. The Kraken normal-mode program developed by Porter¹⁶ is employed herein to predict acoustic propagation in the ocean. The Kraken program, which is one of the most widely used models, efficiently and accurately calculates horizontal wave numbers and mode shape functions for a given acoustic ocean environment.

3.2. Multiple-constraint MVDR-MFP algorithm

The MCMVDR-MFP algorithm calculates an optimal weight vector for the array by using linear multiple constraints. To minimize the impact of element failures, the MCMVDR-MFP algorithm applies additional constraints to MVDR-MFP instead of using a single constraint. These constraints are composed of unity gain for the desired point as in MVDR and zero gain for all the defective elements. For M given constraints, MCMVDR-MFP calculates the optimal weight vector to minimize output power S_{mcmvdr} , while maintaining M constraints as

$$S_{mcmvdr} = w^H R w \text{ subject to } w^H e_1 = d_1, \dots, w^H e_M = d_M \quad (6)$$

where w is the weight vector of MCMVDR-MFP, R is the cross-spectral matrix of the input data for the array, e_i is the constraint vector for the i^{th} constraint point, and d_i is the constraint value for the i^{th} constraint point⁸. Solving Eq. (6) using the Lagrange multiplier method, the weight vector is derived as

$$w_{mcmvdr} = R^{-1} E (E^H R^{-1} E)^{-1} D^H \quad (7)$$

where $E = [e_1 | e_2 | \dots | e_M]$ is the constraint replica matrix and $D = [d_1, d_2, \dots, d_M]^T$ represents the constraint column vector. Finally, by substituting w_{mcmvdr} from Eq. (7) into Eq. (6), the output power for a steering position (r, z) is obtained as

$$S_{mcmvdr} = D (E^H R^{-1} E)^{-1} D^H \quad (8)$$

where S_{mcmvdr} is the detection factor at range r and depth z that indicates the likeliness of detection for a given data set. In this algorithm, selecting suitable constraints for a given environment and system is essential in order to achieve better performance.

Previous research in the literature has provided techniques to enhance beamforming performance using multiple constraints for MVDR-MFP. Multiple neighborhood location constraints^{8, 17} are used to ensure that the mainlobe of the beamformer approximates that of the Bartlett beamformer which is less sensitive to the mismatch. The constraint replica matrix is selected from the replica vectors of a desired point as well as its neighboring points. Environmental perturbation constraints¹⁸ are applied to improve performance to certain environmental uncertainties in the ocean parameters. The constraints are selected to maintain the expected array gain of the minimum variance beamformer by using statistical knowledge of environmental parameter perturbations. This paper presents the multiple linear constraints for MVDR-MFP to contain unity gain for the desired point and zero gain for the defective elements. If we assume that there are L defective elements in the array, the multiple constraints are selected as follows. The e_l is set to the replica vector for the desired point and d_l is set to one to have the unity gain constraint as in MVDR-MFP. The other L sets of e_i and d_i constraints are employed to force zero weights for the L defective elements. For the l^{th} defective element in the array, the l^{th} row of the e_i vector is set to unity and all the other rows of the e_i vector to zero, and the d_i is assigned to zero so that the weight for the l^{th} element can be zero by the

constraint equation, $w^H e_i = d_i$, as expressed in Eq. 6. For instance, if there are defects in the 1st, 3rd, and 4th elements, the constraint replica matrix (E) and constraint vector (D) are given as

$$E = \begin{bmatrix} p_1 & 1 & 0 & 0 \\ p_2 & 0 & 0 & 0 \\ p_3 & 0 & 1 & 0 \\ p_4 & 0 & 0 & 1 \\ \vdots & \vdots & \vdots & \vdots \\ p_n & 0 & 0 & 0 \end{bmatrix}, D = [1 \ 0 \ 0 \ 0]^T \quad (9)$$

where p_j is the j^{th} row of the replica vector for the desired point. This algorithm requires the ability to identify the locations of the faulty elements in the array in order to compensate for them. Hence, the number of columns in the E matrix increases as the number of faulty elements increases. If there are no faulty elements, i.e., only one constraint, the MCMVDR-MFP algorithm is the same as the MVDR-MFP algorithm. As expected, the computational load of MCMVDR-MFP will be considerably increased with the addition of more faulty elements.

3.3. Reduced-rank MVDR-MFP algorithm

For vertical line arrays, a fully spanning aperture is necessary to sufficiently sample the pressure field and provide a unique representation of each mode. The vertical arrays that span only a fraction of the water column degrade beamforming performance due to inadequate sampling of some of the acoustic modes. If the array satisfies the minimum length requirement, the performance is mostly determined by the number of array elements. The rank of the cross-spectral matrix is the same as the number of linearly independent pieces of information or the number of sensors. The number of sensors should be at least equal to the number of propagating modes since it is necessary to obtain a unique representation of each of the propagating modes¹⁹. Therefore, the element failures in a vertical line array can reduce the rank of the CSM, resulting in degraded beamforming performance because of the inaccurate inverse CSM in the MVDR-MFP.

The reduced-rank MVDR-MFP (RRMVDR-MFP) algorithm^{9, 20} is used to compensate for element failures by projecting the array output vectors into a lower dimensional subspace while preserving the signal vectors. Firstly, the CSM is transformed into the eigensubspace and the K subspace preserving signals out of N ($K \leq N$) is selected by using a subspace selection criteria. Next, the reduced subspace is used to calculate the pseudo-inverse of the CSM, optimal weighting vectors, and finally the beamforming output response. By applying an eigen-decomposition method, the CSM is decomposed into a set of eigenvectors and eigenvalues given as

$$R = E[XX^H] = ULU^H = \sum_{i=1}^K \lambda_i u_i u_i^H + \sum_{i=K+1}^N \lambda_i u_i u_i^H \quad (10)$$

where $U = [u_1 | u_2 | \dots | u_n]$ is the orthogonal matrix whose columns are composed of the eigenvectors u_i associated with λ_i and $L = \text{diag}[\lambda_1 \lambda_2 \dots \lambda_n]$ is the diagonal matrix whose diagonal elements consist of the eigenvalues λ_i which are sorted in decreasing order ($\lambda_1 \geq \lambda_2 \geq \dots \geq \lambda_n$). As shown in Eq. (10), the CSM is divided into two summation terms of the eigenvectors and eigenvalues where the first term is composed of the signal eigenvectors associated with the K largest eigenvalues and the other consists of the noise eigenvectors corresponding to the $(N-K)$ smallest eigenvalues. When there are faulty elements in the array, the noise vectors corresponding to the least significant eigenvalues are dominant in MVDR-MFP and degrade the spectral output of the MVDR-MFP beamformer. RRMVDR-MFP excludes the noise

eigenvectors corresponding to the least significant eigenvalues and reduces the rank of the CSM from N to K . Thus, the formation of the weight vector for RRMVDR-MFP is calculated as

$$w_{rrmvdr} = \frac{\sum_{i=1}^K \frac{1}{\lambda_i} (u_i^H p) u_i}{\sum_{i=1}^K \frac{1}{\lambda_i} |u_i^H p|^2} \quad (11)$$

where p is the replica vector and K is the rank of the reduced CSM. The final spectral output of RRMVDR-MFP is given by:

$$S_{rrmvdr} = \frac{1}{\sum_{i=1}^K \frac{1}{\lambda_i} |u_i^H p|^2} \quad (12)$$

RRMVDR-MFP can achieve enhanced robustness by excluding noise vectors distorted by the element failures and environmental mismatches. Several algorithms for determining the reduced-rank approximation have been introduced to enhance beamforming performance when there are environmental mismatches^{10, 11, 20}. The signal power threshold method selects the eigenvectors associated with eigenvalues containing a large fraction of total power given by

$$\frac{\lambda_i}{\text{trace}(R)} \geq \gamma \quad (13)$$

where trace represents the sum of all diagonal elements of a matrix and γ is the threshold value necessary to preserve signal power¹⁰. The signal coherence method can be employed to choose the eigenvectors corresponding to eigenvalues that have large enough correlation with the replica vector for each search location given by

$$|u_i^H p|^2 \geq \delta^2 \quad (14)$$

where δ^2 is the constraining value that can be used to select an eigenvector belonging to the signal subspace¹¹. This method creates additional computational load to calculate the correlation between replica vectors and eigenvectors for every steering point in a large search region. Thus, the power threshold method is herein used as the subspace selection criteria since it is computationally more efficient than the signal coherence method. The strength of RRMVDR-MFP is that it can be employed without knowing the physical locations of the faulty sensors, and its computational complexity is not increased as the number of defective elements increases. Thus, this method promises to require a lower computational load as compared to other fault-tolerant algorithms such as MCMVDR-MFP.

3.4. Compensated MVDR-MFP algorithm

The compensated MVDR matched-field processing (CMVDR-MFP) algorithm reconstructs the data for the faulty nodes by using a linear prediction algorithm with the data available from neighboring sensors that are non-faulty. The MVDR-MFP algorithm is then applied to obtain final beamforming outputs. The farfield data of a point source in shallow water waveguides using the normal modes can be modeled by the Prony method that is used to model data for equally spaced samples by the linear combination of damped exponentials²¹. It is assumed that L sensors are defective in the array where each sensor is equally spaced

and the faulty sensors have been identified. The data for the faulty sensors are interpolated by the linear prediction algorithm. The p^{th} -order forward prediction for the k^{th} defective sensor data is obtained by

$$\hat{X}_k^f = \sum_{j=1}^P X_{k-j} a_j, P+1 \leq k \leq M \quad (15)$$

and the backward prediction for the k^{th} defective sensor data is given by

$$\hat{X}_k^b = \sum_{j=1}^P X_{k+j} a_j^*, 1 \leq k \leq M-P \quad (16)$$

where P is the order of the linear prediction, M is the number of signals, a_j is the linear prediction coefficient corresponding to the i^{th} sensor apart from the faulty sensor, and X_j is the signal of the j^{th} sensor^{22,23}. The data for the k^{th} faulty sensor is estimated from a linear combination of the forward and backward predictions given by

$$\hat{X}_k = \alpha \hat{X}_k^f + (1-\alpha) \hat{X}_k^b, \alpha \in [0, 0.5, 1] \quad (17)$$

where α is the weighting constant of the forward and backward predictions whose value depends on whether one or both predictions are available. If there is no forward prediction for faulty nodes located near the top end of the array, the weighting constant is zero. If there is no backward prediction for faulty nodes located near the bottom end of the array, the weighting constant is one. Otherwise, the weighting constant is 0.5 when both predictions are available.

The linear prediction coefficients a_j are calculated using the Burg algorithm which is based on forward and backward prediction errors and estimates the reflection coefficients²⁴. The Burg method is widely employed to predict missing data in beamforming applications and provides an unbiased estimate even though the number of data points is small^{22,23}. The interpolation process to estimate the faulty data can not be applied unless there is at least one segment of $P+1$ consecutive working sensors in the array. In the worst case, a configuration of $B \leq \lfloor N/(P+1) \rfloor$ faulty elements can be used to meet this minimum requirement. For example, for $N=32$, and $P=10$, the maximum number of faulty nodes estimated by the Burg algorithm is two. P should be chosen based on the trade-off between accuracy and time lag since low order generates smoothed estimates, and high order provides spurious peaks and large variance estimates. Thus, an appropriate linear prediction order for the Burg algorithm is selected by using past experience and experiments when necessary. The computational load of the CMVDR-MFP increases as the number of faulty nodes increases since the frequency of linear predictions to estimate the data for faulty nodes is increased.

4. Computational Complexity of Fault-tolerant MFP Algorithms

The proposed fault-tolerant algorithms might present additional computational cost compared to the MVDR-MFP algorithm in order to achieve the necessary improved performance. The additional computational cost results in more implementation difficulties in real-time sonar applications. In this section, the computational complexities and execution times are investigated to determine whether they can be reasonably employed on a real-time implementation on sonar array systems. The computational complexities for the fault-tolerant MVDR-MFP algorithms are shown in Table 1 where N is the number of nodes, R is the number of range points, and D is the number of depth points. F is the number of faulty elements, K is the rank of the reduced CSM, and P is the order of the linear prediction algorithm.

As shown in Table 1, in the MVDR-MFP algorithm which uses a fixed number of data points per sensor, the FFT stage for all sensor nodes requires a computational complexity of $O(N)$. The CSM stage has a complexity of $O(N^2)$ and the inversion of the CSM matrix using the Gauss Jordan elimination method involves a complexity of $O(N^3)$. The steering stage has a complexity of $O(RDN^2)$ for a single narrowband frequency^{25,26}. In the MCMVDR-MFP algorithm, the computational complexities of all stages except the steering stage are the same as those of MVDR-MFP. The steering stage involves F times higher complexity than that of MVDR-MFP. The eigen-decomposition and steering stages of the RRMVDR-MFP algorithm require $O(N^3)$ and $O(RDNK)$ respectively since RRMVDR-MFP uses an eigen-decomposition method to transform the CSM into eigensubspace instead of using matrix inversion. The CMVDR-MFP algorithm adds a complexity of $O(FP^2)$ for the linear prediction stage because the linear prediction is required to reconstruct the data for faulty nodes. As the number of defective sensors increases, the computational load for the MCMVDR-MFP and CMVDR-MFP algorithms is increased but not for the RRMVDR-MFP algorithm. From these results, it might be expected that the fault-tolerant algorithms will increase computational complexity as compared to the MVDR-MFP baseline, but the degree of increase will depend on implementation details. The computational complexity of MCMVDR-MFP is higher than that of the other fault-tolerant algorithms since the complexity of the steering stage is most computationally dominant.

Table 1. Computational complexities of fault-tolerant MFP algorithms.

	MVDR	MCMVDR	RRMVDR	CMVDR
FFT	$O(N)$	$O(N)$	$O(N)$	$O(N)$
Linear Prediction	—	—	—	$O(FP^2)$
CSM	$O(N^2)$	$O(N^2)$	$O(N^2)$	$O(N^2)$
Inversion or Eigen-decomposition	$O(N^3)$	$O(N^3)$	$O(N^3)$	$O(N^3)$
Steering	$O(RDN^2)$	$O(RDFN^2)$	$O(RDNK)$	$O(RDN^2)$

Fig. 2 shows the execution times of the fault-tolerant algorithms measured using Matlab 6.0 on a personal computer with Windows XP and a 2.0 GHz Pentium 4. The average execution time of each computational stage per iteration was measured for several hundreds of iterations to obtain the execution time for one beamforming iteration more accurately. The number of sensors is 32 and the number of range and depth grid points is 40 and 80 respectively. The order of the linear prediction is ten and the number of faulty nodes is varied from zero to ten where the faulty nodes are distributed from the top end of the array toward the bottom end with a faulty-node spacing of one. As expected from the results in Table 1, it is seen that the execution times of MCMVDR-MFP and CMVDR-MFP increase as the number of defective sensors increases. In particular, as the number of faulty nodes increases, the execution time of MCMVDR-MFP is much higher than that of the other fault-tolerant algorithms since the execution time is increased significantly in the steering stage. The RRMVDR-MFP algorithm is confirmed to be most computationally efficient of the fault-tolerant algorithms for a given problem size.

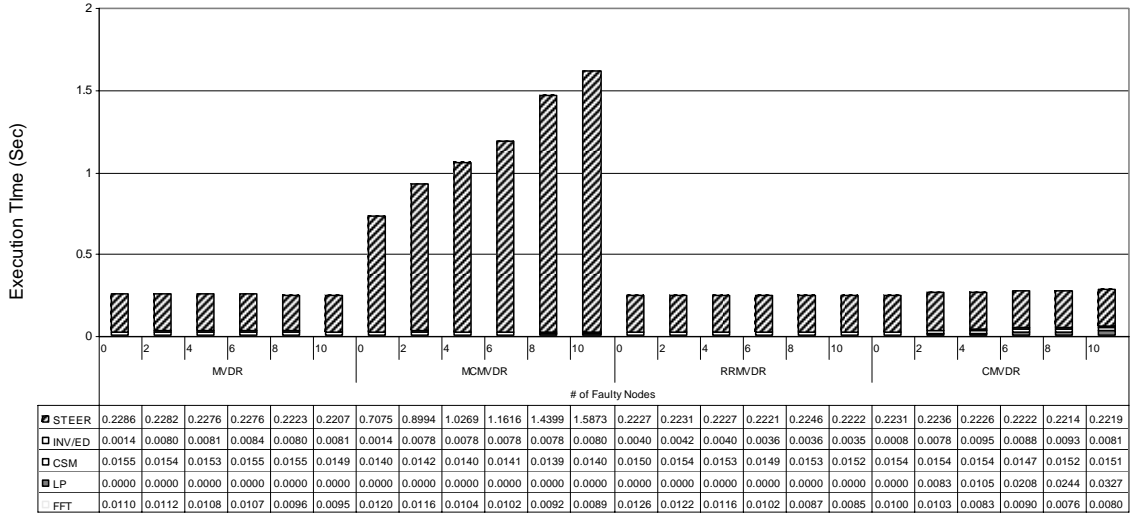


Fig. 2. Execution time per iteration.

5. Simulation and Performance Analysis

In this section, performance of the fault-tolerant MVDR-MFP algorithms is analyzed in terms of the number of faulty elements, their positions, and signal-to-noise ratios. The testbed environment used in this simulation is the same as that described in Section 4. The peak-to-background ratios for various faulty-node configurations were calculated from 50 independent trials of the noise and faulty-node position. For a given set of environmental and system parameters, the final beamforming output is commonly depicted as an ambiguity surface indicating the likeliness of target detections in which peak positions imply the locations that are most likely to be targets. In order to provide a means of quantifying characteristics of the ambiguity surface, the peak-to-background ratio is defined as $PBR = (p - \mu) / \mu$ where p is the peak value and μ is the mean background level which is calculated by excluding a small number of points around the peak. PBR is extensively used as a concrete performance metric in beamforming applications^{9, 20}. A higher PBR implies that performance of source localization is better. The CMFP and MVDR-MFP algorithms are used as baselines for comparing the performance of the three fault-tolerant algorithms.

In this simulation, the pressure field data was generated by the Kraken normal mode model for a point source which is located at 60 m in depth and 10 km in range, and has 200 Hz frequency and 10 propagating modes. The vertical line array contains 32 hydrophones spaced at 3 m apart from 10 m to 103 m in depth. The noise for each hydrophone contains a Gaussian distribution with zero mean and SNR of -10 dB and 10 dB. The simulation parameters are a single frequency bin, 40 grid points in range, 80 grid points in depth, and up to ten faulty nodes.

Fig. 3 shows the ambiguity surfaces of MVDR-MFP and the three fault-tolerant MVDR-MFP algorithms when there are defects at the 16th, 18th, and 20th sensors with SNR of 10 dB. It is demonstrated that the CMFP algorithm localizes the position of the source exactly at 60 m in depth and 10 km in range, but generates much higher sidelobe levels and background noises than the other fault-tolerant algorithms. The MVDR-MFP algorithm is implemented using the diagonal loading method that adds white noise to the diagonal elements of the CSM to reduce the inaccuracy of the CSM inversion. MVDR-MFP also localizes

the source at the exact position but obtains higher background noises due to element failures. As depicted in Fig. 3 (c)-(e), the three fault-tolerant MVDR-MFP algorithms achieve better localization performance than MVDR-MFP. The ambiguity surface alone is not enough to infer the statistical behavior of algorithms since it indicates goodness of the beamforming outputs. Thus, PBR of the fault-tolerant algorithms is compared in terms of number of faulty nodes and faulty configurations in the following.

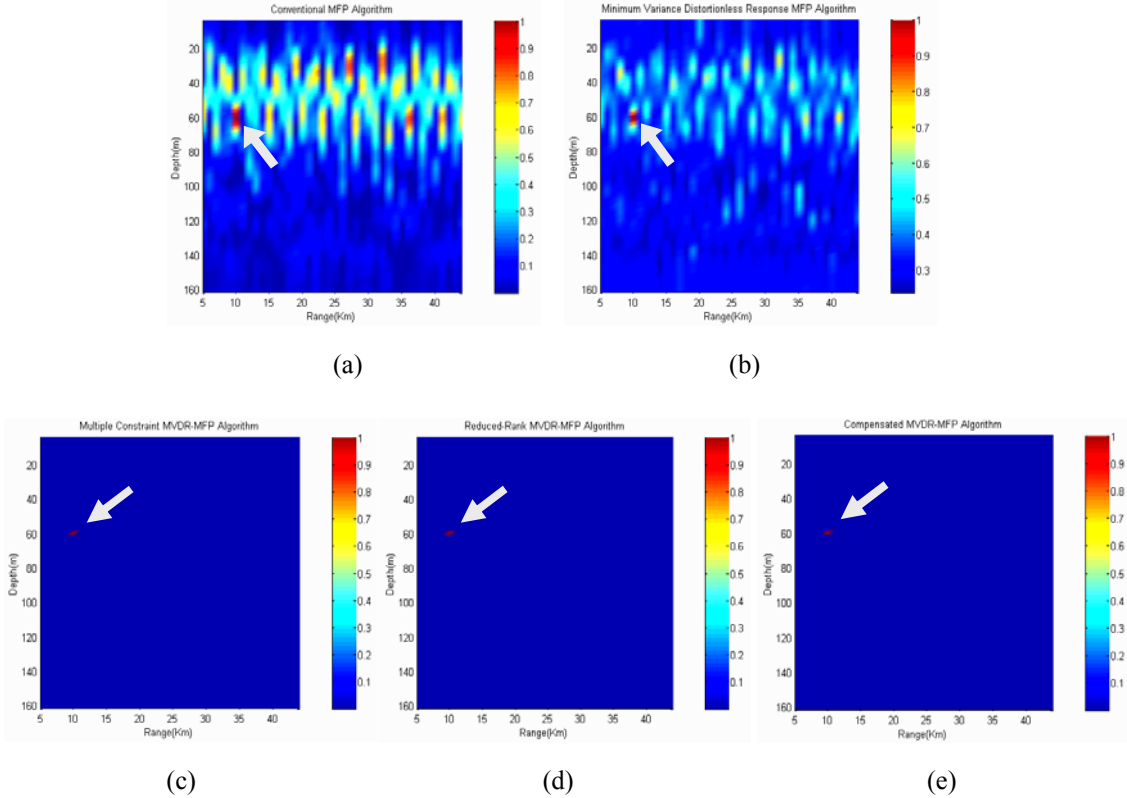


Fig. 3. Ambiguity surfaces of CMFP (a), MVDR-MFP (b), MCMVDR-MFP (c), RRMVDR-MFP (d), and CMVDR-MFP (e) algorithms.

In this section, four faulty-node configurations (i.e. top-end, bottom-end, center, and random) are used to examine the features of the fault-tolerant algorithms for various failure distributions in the vertical line array. The top-end configuration means that there are faulty nodes equally distributed from the top-end toward the bottom-end according to a given space between two faulty nodes. For instance, the 1st, 3rd, 5th, and 7th nodes are defective when the number of faulty nodes is four and the faulty-node spacing is two in the top-end configuration. By contrast, in the bottom-end configuration, faulty nodes are located from the bottom-end toward the top-end. In the center configuration, the faulty nodes are distributed from the center node toward both ends of the vertical line array with specified faulty-node spacing. The 16th, 18th, and 20th nodes are faulty in the center configuration where the number of faulty nodes is three and the spacing distance is two. The random configuration denotes that faulty nodes are randomly distributed at any position in the array as many as a given number of defective elements.

PBR of the fault-tolerant MVDR-MFP algorithms is depicted in Fig. 4 in terms of the four faulty-node configurations with a faulty-node spacing of one, SNR of 10 dB, and up to ten faulty nodes. PBR of

MVDR-MFP depends on the magnitude of the mismatch presented by the faulty nodes, but the fault-tolerant algorithms prove to be less sensitive to this mismatch. For instance, as the number of faulty nodes increases, the PBR of MVDR-MFP in the center configuration rapidly decreases since the center nodes produce higher mismatch due to the strong intensity of pressure fields as depicted in Fig. 1. MCMVDR-MFP and RRMVDR-MFP algorithms achieve better beamforming performance than the other fault-tolerant algorithms for the given defective elements. RRMVDR-MFP achieves a slightly higher PBR in some cases even though the number of defective elements increases because performance of the RRMVDR-MFP algorithm is affected by its specified power threshold level. A small power threshold level is sensitive to the additive noise but obtains higher PBR because it can preserve signal vectors and large noise vectors as well in the reduced subspace. By contrast, a large power threshold level is robust to the additive noise but obtains lower PBR because it filters out the noise vectors as well as small signal vectors in the reduced subspace. In Fig. 4, a relatively small power threshold level, which is -80 dB of the total power of the CSM, is used to obtain a higher PBR as small fluctuations in the PBR can be considered insignificant. The PBR of CMVDR-MFP is also slightly increased in some cases as the number of defective elements increases since results of the linear prediction algorithm are affected by the additive noises in the sensors. However, MCMVDR-MFP obtains steady performance as the number of faulty nodes increases up to ten. Finally, as the number of faulty nodes increases, the PBR of CMVDR-MFP rapidly decreases since the results of the linear prediction algorithm are highly degraded with a large number of burst faulty nodes.

Fig. 5 illustrates the PBR of these algorithms in terms of the same configurations but in this case with -10 dB SNR. As SNR decreases, the PBR of the fault-tolerant algorithms decreases as expected. The performance of the fault-tolerant algorithms with SNR of -10 dB follows almost the same trends as in Fig. 4.

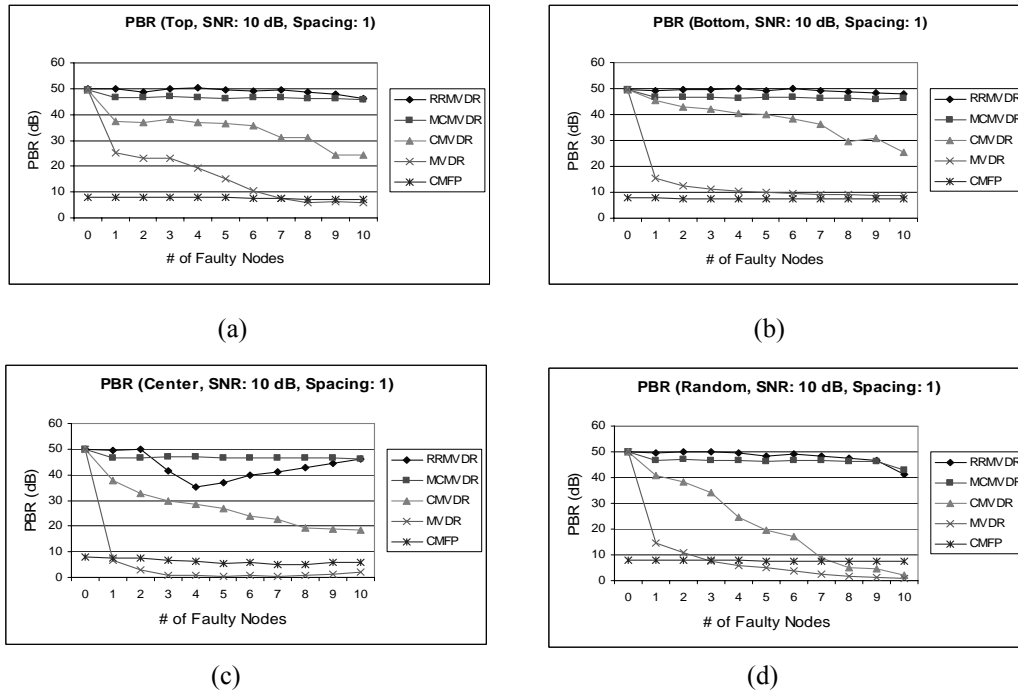


Fig. 4. Peak-to-background ratios with SNR of 10 dB and faulty-node spacing of one in top-end (a), bottom-end (b), center (c), and random (d) configurations.

The PBR is depicted in Fig. 6 but in this case in terms of a faulty-node spacing of two. The order of the linear prediction is ten and the SNR is 10 dB. With a faulty-node spacing of two, PBR performance of all the fault-tolerant algorithms follows the same trends as with a faulty-node spacing of one except in CMVDR-MFP. PBR of CMVDR-MFP more rapidly decreases in the center configuration of faulty nodes. The reason is that the Burg algorithm requires at least one segment of 11 consecutive working nodes to estimate the data for faulty nodes, but this configuration does not provide a segment of 11 consecutive working nodes as the number of faulty nodes increases. When the number of faulty nodes is small in the top-end, bottom-end, and center configurations, CMVDR-MFP shows higher PBR since the results of linear prediction are better than those in the burst faulty-node configurations.

Fig. 7 shows PBR where simulation parameters are the same as those in Fig. 6 with exception of -10 dB SNR. As SNR decreases, PBR of the fault-tolerant algorithms highly decreases as in Fig. 5. Although scaled downward, the performance trends of the fault-tolerant algorithms with the SNR of -10 dB are generally the same as in Fig. 6.

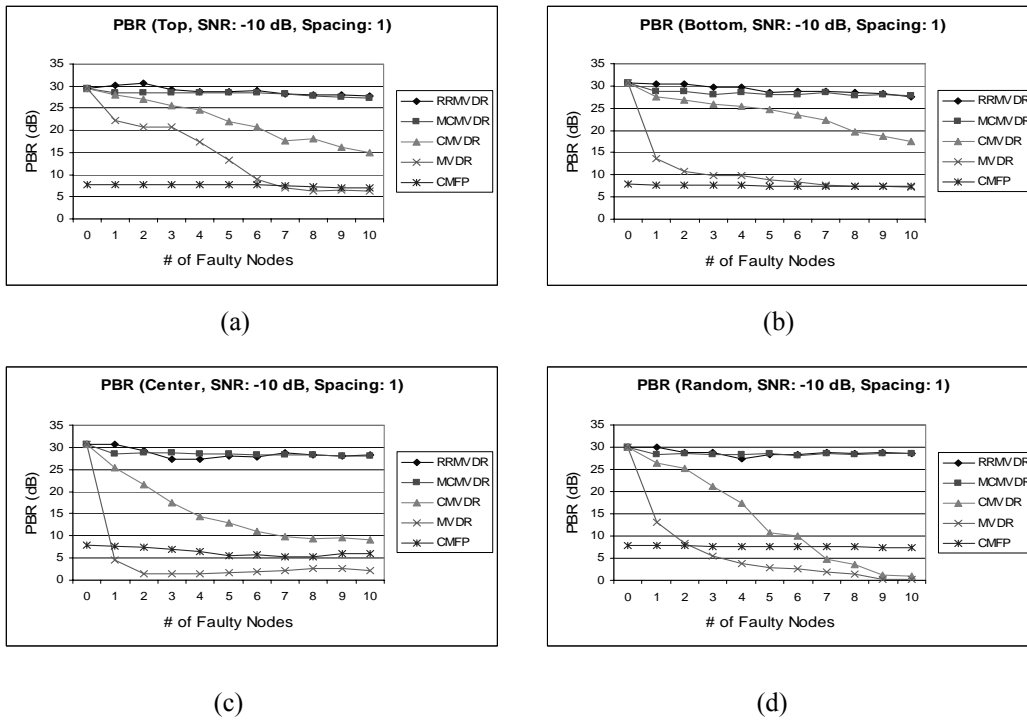


Fig. 5. Peak-to-background ratios with SNR of -10 dB and faulty-node spacing of one in top-end (a), bottom-end (b), center (c), and random (d) configurations.

6. Conclusions

Element failures in sonar arrays positioned in severe undersea environments seriously degrade beamforming performance of adaptive algorithms since such element failures generate a highly distorted beam pattern and increased sidelobe level. In this paper, the effects of element failures for the MVDR-MFP algorithm are analyzed in terms of signal-to-noise ratios, the number of faulty elements, and their positions. Three fault-tolerant MFP algorithms are developed to determine which fault-tolerant algorithms

perform best in the presence of element failures by examining their performance trade-offs in terms of computational complexity, ambiguity surface, and peak-to-background ratio.

The impacts on beamforming performance caused by element failures are analyzed by using the power ratio. The results demonstrate that the effects of element failures in the conventional and MVDR-MFP algorithms are increased as the number of faulty nodes increases. The power ratios are also lowered with increased signal-to-noise ratios. The effects of defective sensors in strong pressure fields on the array are higher than those of defective sensors in weak pressure fields. The power ratio depends on range and depth of the source because the pressure field intensity for each element from the source varies according to the position of the source.

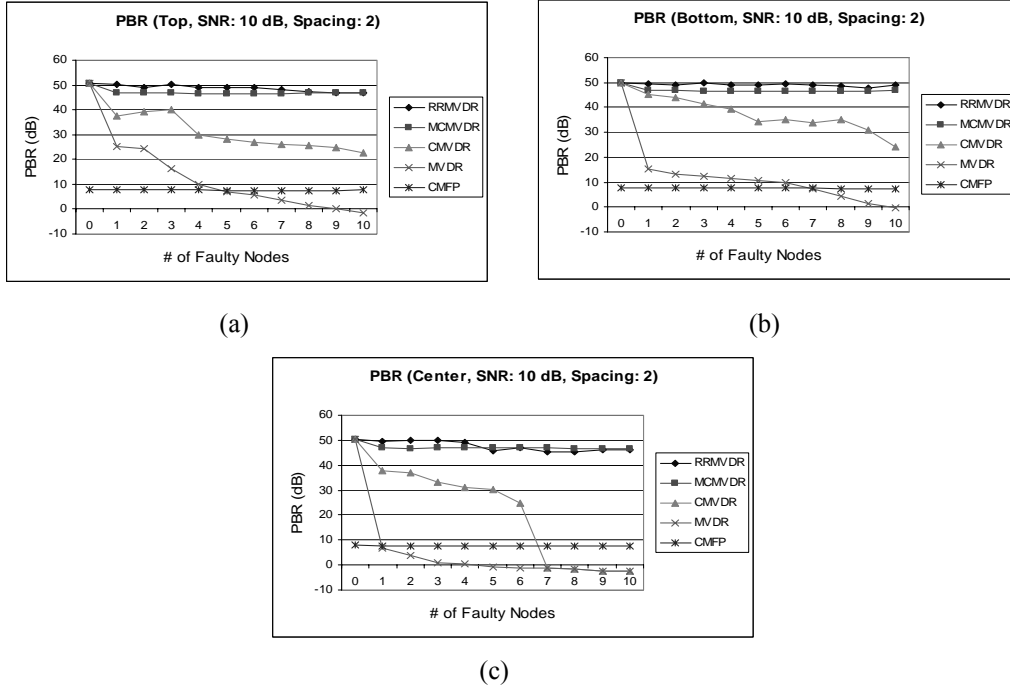


Fig. 6. Peak-to-background ratios with SNR of 10 dB and faulty-node spacing of two in top-end (a), bottom-end (b), and center (c) configurations.

The MCMVDR-MFP algorithm achieves promising fault tolerance by adjusting the gains for faulty nodes to zero to mitigate their effects. The RRMVDR-MFP algorithm enhances robustness to element failures by projecting the array output vectors into a lower dimensional subspace while preserving signal vectors. The CMVDR-MFP algorithm obtains better beamforming performance in the presence of a small number of faulty nodes by reconstructing the data for faulty nodes with the available data from neighboring working elements using a linear prediction algorithm. The performance results demonstrate that the three fault-tolerant algorithms achieve higher fault tolerance than MVDR-MFP in the presence of element failures. RRMVDR-MFP and MCMVDR-MFP algorithms obtain better performance than the other algorithms. However, the MCMVDR-MFP and CMVDR-MFP algorithms require the ability to locate the defective sensors while this is not necessary for the RRMVDR-MFP algorithm. RRMVDR-MFP is computationally more efficient than the other fault-tolerant algorithms whose computational complexities are increased as the number of faulty nodes increases. Given the increasing demands for reliable

algorithms for future sonar systems, these fault-tolerant algorithms provide a feasible solution for real-time and fault-tolerant implementation of beamforming algorithms on distributed array systems.

For future work, the fault-tolerant MFP algorithms presented in this paper can be extended to compensate for the performance degradation generated by other environmental and system mismatches. Fault-tolerant MFP algorithms have presented a significant increase in computational complexity that makes development and use of high-performance systems imperative in real-world applications. The fault-tolerant algorithms need to be integrated with advanced parallel processing algorithms and architectures to provide efficient fault-tolerant parallel processing methods that assure high reliability and meet the real-time requirements of distributed sonar systems in spite of processing and sensor failures.

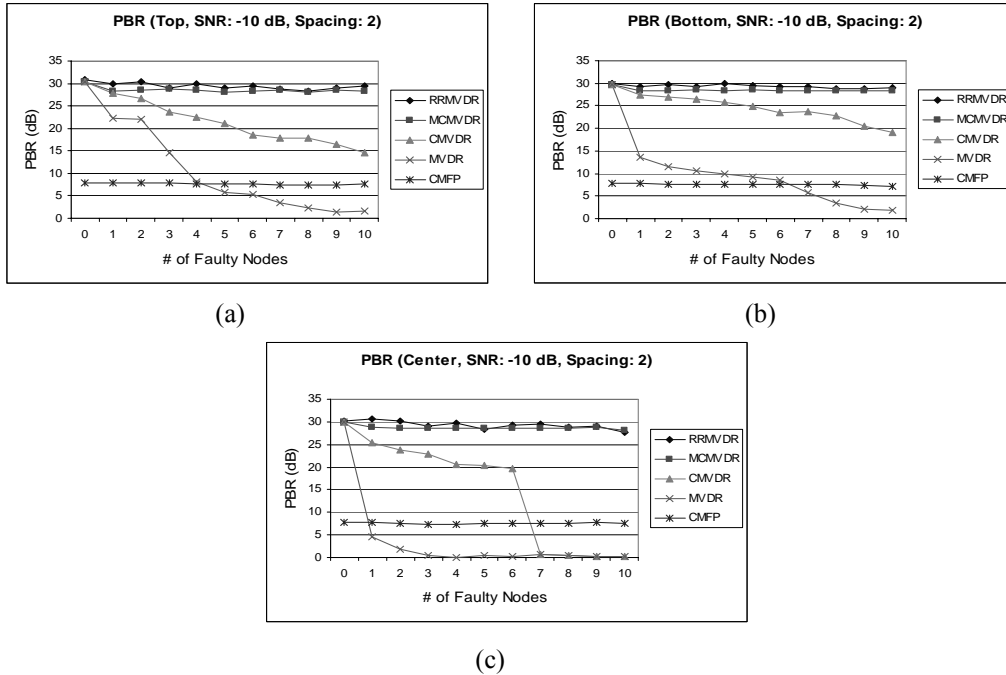


Fig. 7. Peak-to-background ratios with SNR of -10 dB and faulty-node spacing of two in top-end (a), bottom-end (b), and center (c) configurations.

Acknowledgements

We acknowledge and appreciate the support for this work provided by the Office of Naval Research on grant N00014-99-10278. Special thanks go to Byung Il Koh in the HCS Lab at the University of Florida for his many useful suggestions.

References

1. A. Baggeroer, W. Kuperman, and H. Schmidt, "Matched-field processing: Source localization in correlated noise as an optimum parameter estimation problem," *J. Acoust. Soc. Am.* **83** (2), 571-587 (1988).
2. B. Yeo and Yilong Lu, "Array failure correction with a genetic algorithm," *IEEE Trans. on Antennas and Propagation* **47** (5), 823-828 (1999).

3. W. Rosen and A. George, "Fault tolerance in autonomous acoustic arrays," *J. of the Franklin Institute* **336B**, 19-32 (1999).
4. D. Ramsdale and R. Howerton, "Effect of element failures and random errors in amplitude and phase on the sidelobe level attainable with a linear array," *J. Acoust. Soc. Am.* **68** (3), 901-905 (1980).
5. M. H. Er and S. K. Hui, "Beamforming in the presence of element failures," *Electronics Letters* **27** (3), 273-275 (1991).
6. T. Gee, K. Pepe, R. Collier, K. Everman, E. Freer, R. Wetherington, and G. Tarasek, "Compensation for missing sensors in a real-time measurement beamforming system," *IEEE Oceans '97 Conference Proceedings*, 351-357 (1997).
7. R. Mailloux, "Array failure correction with a digitally beamformed array," *IEEE Trans. On Antennas and Propagation* **44** (12), 1543-1550 (1996).
8. H. Schmidt and A. Baggeroer, "Environmentally tolerant beamforming for high resolution matched field processing: deterministic mismatch," *J. Acoust. Soc. Am.* **88** (4), (1990).
9. J. Ozard and G. Brooke, "Improving performance for matched-field processing with a minimum variance beamformer," *J. Acoust. Soc. Am.* **91** (1), 141-150 (1992).
10. H. Cox and R. Pitre, "Robust DMR and multi-rate adaptive beamforming," *Thirty-First Asilomar Conference on Signals, Systems, and Computers* **1**, 920-924 (1997).
11. N. Lee, L. Zurk, and J. Ward, "Evaluation of reduced-rank, adaptive matched-field processing algorithms for passive sonar detection in a shallow-water environment," *Thirty-Third Asilomar Conference on Signals, Systems, and Computers* **2**, 24-27 (1999).
12. G. Fricther, C. Byrne, and C. Feuillade, "Sector-focused stability methods for robust source localization in matched-field processing," *J. Acoust. Soc. Am.* **88** (6), 2843-2851 (1990).
13. D. Gingras, "Methods for predicting the sensitivity of mismatched-field processors to mismatch," *J. Acoust. Soc. Am.* **86** (5), 1940-1949 (1989).
14. M. Porter, "KRAKEN normal-mode program," http://oalib.saic.com/modes/acousticstoolbox/manual_html/kraken.html, (1997).
15. M. Porter, "Acoustic models and sonar systems," *J. of Oceanic Engineering* **18** (4), 425-437 (1993).
16. M. Porter, "The KRAKEN normal-mode program," SACLANT Memorandum, SM-245, (1991).
17. J. Krolik, "Robust matched-field beamforming with benchmark shallow-water acoustic array data," *IEEE Proceedings, ICASSP-96* **2**, 1185-1188 (1996).
18. J. Krolik, "Matched-field minimum variance beamforming in a random ocean channel," *J. Acoust. Soc. Am.* **92** (3), 1408-1419 (1992).
19. S. Tantum and L. Nolte, "On array for matched-field processing," *J. Acoust. Soc. Am.* **107** (4), 2101-2111 (2000).
20. C. Byrne and R. Brent, "A stable data-adaptive method for matched-field array processing in acoustic waveguides," *J. Acoust. Soc. Am.* **87** (6), 2493-2502 (1990).
21. E. Shang, H. Wang, and Z. Huang, "Waveguide characterization and source localization in shallow water waveguides using the Prony method," *J. Acoust. Soc. Am.* **83** (1), 103-108 (1988).
22. J. Fulton, "Smoothing approaches to reconstruction of missing data in array processing," *Proc. US/Australia Joint Workshop on Defense Applications of Signal Processing*, Elsevier, 87-94, (2001).
23. D. Swinger, R. Walker, "Line-array beamforming using prediction for aperture interpolation and extrapolation," *IEEE Trans. on Acoustics, Speech, and Signal Processing* **37** (1), 16-30 (1989).
24. P. Stoica and R. Moses, "Introduction to spectral estimation," Prentice Hall, New Jersey, (1997).
25. K. Cho, A. George, R. Subramanian, and K. Kim, "Parallel algorithms for adaptive matched-field processing on distributed array systems," *J. of Computational Acoustics* **12** (2), 149-174 (2004).

26. P. Sinha, A. George, and K. Kim, "Parallel algorithms for robust broadband MVDR beamforming," *J. of Computational Acoustics* **10** (1), 69-96 (2002).